

Multiple Deformation Mechanisms of a Metastable β Ti-V Alloy at High Strain Rates

Wang Qiaochu, Hui Songxiao, Ye Wenjun, Liu Rui, Yu Yang

State Key Laboratory for Fabrication & Processing of Nonferrous Metals, General Research Institute for Nonferrous Metals, Beijing 100088, China

Abstract: Dynamic compressive properties, microstructure evolution and deformation modes of binary Ti-16V alloys have been investigated. Mechanical tests were performed on the split Hopkinson pressure bar. In addition, optical microscopy, electron backscatter diffraction technique and transmission electron microscopy were applied to observe deformed microstructures. The results show that flow stress and strain hardening rate are both insensitive to loading strain rates. Critical instability strain rate of Ti-16V alloys is measured to be about 3000 s^{-1} . $\{332\}\langle 113 \rangle$ type mechanical twinning and stress induced ω phase transformation are dominant dynamic deformation modes of Ti-16V alloys. Schmid factor, calculated by the twinning Schmid factor model, is proved to be a key parameter determining the activation of twinning behavior of Ti-16V alloys.

Key words: metastable β titanium alloy; dynamic deformation; deformation mode; twinning

Over the past few decades, a diverse range of metastable β titanium alloys have been rapidly developed due to their excellent biocompatibility, shape memory effect, deformability and super elasticity^[1-3]. These superior features have been found to be sensitive to alloy composition^[4]. For metastable β titanium alloys, the deformation mode is significantly influenced by the phase stability governed by element content. With a decrease of β phase stability, a transition of dislocation slip to mechanical twinning and stress induced phase transformation may occur^[5]. The relationship between deformation mode and phase stability could be described by the Bo-Md diagram^[6].

Deformation modes of metastable β titanium alloys are recognized to be complex, such as $\{332\}\langle 113 \rangle$ and/or $\{112\}\langle 111 \rangle$ type twinning, stress induced phase transformation and dislocation slip^[7]. Kuan et al observed plate-shaped stress induced ω phase and wavy slip in tensile microstructures of Ti-15.8V and Ti-19.9V alloys^[8]; Oka and Taniguchi showed the experimental evidence of $\{332\}\langle 113 \rangle$ type twinning in cold rolled Ti-15.5V alloys^[9]; Hanada and Izumi explained the relationship between $\{332\}\langle 113 \rangle$ type twin-

ning and stress induced ω phase in Ti-16~22V alloys, which indicated that stress induced ω phase is preferentially induced in $\{332\}\langle 113 \rangle$ type twinning^[10]; Wang et al reported that the deformation modes of Ti-16~22V alloys changed from plate-shaped stress induced ω phase transformation with the habit plane of $\{5052\}$ to $\{332\}\langle 113 \rangle$ type mechanical twinning^[11]; Koul and Breedis found stress induced α' phase with hexagonal close packing structure in deformed Ti-16V alloys^[12]. Above all, twinning and stress induced phase transformation were verified to be dominant quasi-static deformation mechanisms of metastable Ti-V alloys but dynamic deformation modes are rarely reported.

Dynamic mechanical response of metals may be quite different from those deformed at a quasi-static strain rate. Generally, flow stress increases with increasing strain rate. For example, Ti-15V-3Sn-3Al-3Cr alloys have a strain rate hardening behavior^[13]. Of course, a strain rate softening behavior was observed in other materials, like TRIP/TWIP steel with high content of manganese^[14]. A lot of studies on dynamic deformation modes of titanium alloys were also conducted. Ahmed et al showed that an increase of strain rates

Received date: May 15, 2018

Foundation item: National Natural Science Foundation of China (51601016)

Corresponding author: Liu Rui, Ph. D., State Key Laboratory for Fabrication & Processing of Nonferrous Metals, General Research Institute for Nonferrous Metals, Beijing 100088, P. R. China, Tel: 0086-10-60662663, E-mail: h_o_n_o_r@163.com

Copyright © 2019, Northwest Institute for Nonferrous Metal Research. Published by Science Press. All rights reserved.

from 10^{-3} to 10^2 s^{-1} leads to a restriction of stress induced phase transformation and a proliferation of twins^[15]. Zhan et al observed multiple deformation mechanisms including $\{332\}\langle 113 \rangle$ and $\{112\}\langle 111 \rangle$ type twinning, stress induced phase transformation and dislocation slip in dynamically deformed microstructures of metastable Ti-Nb alloys^[5]. Note that the activation of twinning depends strongly on the tensile or compression direction with respect to the crystal orientation but the relationship was still unknown.

In this work, metastable Ti-16V alloys were taken as research materials. Dynamic compressive tests were performed to measure mechanical properties. Microstructure evolution and multiple deformation modes were observed and investigated. A calculation model of twinning Schmid factor (SF) was established to show the importance of SF to the predication of deformation modes.

1 Experiment

The Ti-16V alloys were prepared by non-consumable vacuum arc melting using high purity Ti and electrolytic vanadium. The chemical composition is presented in Table 1. The cast ingot was hot rolled, solution treated at 993 K for 1 h and then quenched in water. The samples with a height and diameter of 5 mm for compressive tests were cut from the plates along the rolling direction by electrical discharge machining. Dynamic compressive tests were carried out on the split Hopkinson pressure bar (SHPB). Specimens for optical microscope (OM) observations on Zeiss Axiovert 200Mat were wet ground using silicon carbide papers, polished in SiO_2 suspension liquid and etched in a solution (16 mL distilled water, 3 mL nitric acid and 1 mL hydrofluoric acid). The samples for electron backscatter diffraction (EBSD) analysis performed on JSM-7001F were polished in the OPS solution for 30 min. The transmission electron microscopy (TEM) samples were dryly ground and twinjet polished in another solution (45 mL perchloric acid, 105 mL butyl alcohol and 350 mL methanol) at 50 V and 243 K. TEM observations were performed on the JEM-2010 microscope.

2 Results and Discussion

2.1 Phase stability

Deformation modes of metastable titanium alloys are significantly influenced by β phase stability^[11], which can be predicted by the $\overline{\text{Bo-Md}}$ law. Bo is bond order evaluating the covalent bond strength between Ti and other alloying elements; Md presents the d-orbital energy level of titanium alloys. The average Bo and Md of Ti-16V alloy were calculated to be 2.792 and 2.360, respectively^[16, 17]. Fig.1a shows the location of Ti-16V alloy in the Bo-Md diagram. Note that the location was in the “twinning region” and “ $\beta+\omega$ phase zone”. The inverse pole figure (IPF) of the water quenched sample is exhibited in Fig.1b, showing the equiaxed microstructure with average grain size of 163 μm . In addition to the β phase, quenched ω phase was also observed (see Fig.1c).

2.2 Mechanical response

Dynamic mechanical curves of Ti-16V alloys are shown in Fig.2. The loading strain rates were chosen to be $1000\sim 3700 \text{ s}^{-1}$, in which adiabatic shear band (ASB) and fracture formed. It was found that the strain hardening effect was featured in each curve. Different from α titanium alloys, the work hardening behavior was not common in β -Ti with adequate slip systems. Chichilia et al pointed that twin-dislocation intersections play a significant role in strain hardening behaviors, although dislocation motion accounts for the majority of dynamic deformations^[18]. For metastable β titanium alloys, multiple deformation products probably intersected with each other, which may contribute to the strain hardening effect. It was also found that the rates of strain hardening at different strain rates were nearly identical, which was resulted from the fact

Table 1 Chemical composition of the Ti-16V alloy (wt%)

V	C	O	N	H	Fe	Ti
15.54	0.01	0.025	0.003	0.001	0.025	Bal.

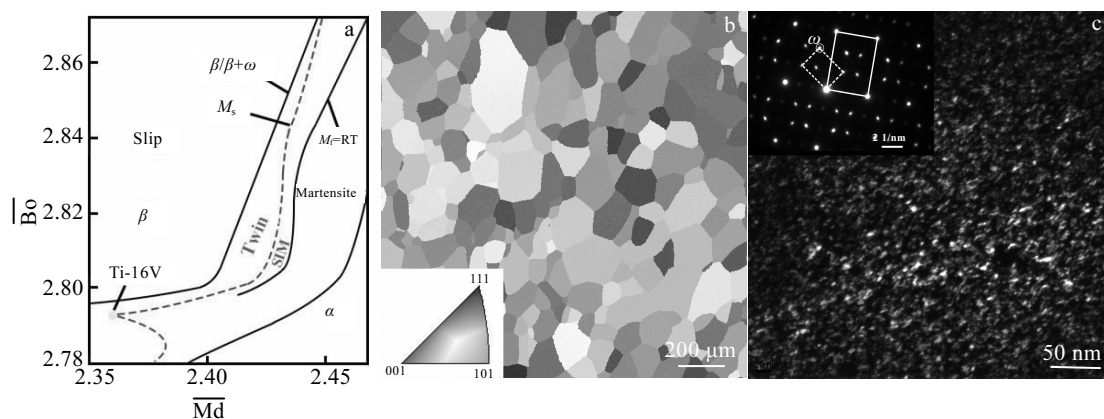


Fig.1 $\overline{\text{Bo-Md}}$ diagram showing the location of Ti-16V alloy (a), EBSD IPF of the water quenched Ti-16V alloy (b), and TEM dark-field image of quenched ω phase (c)

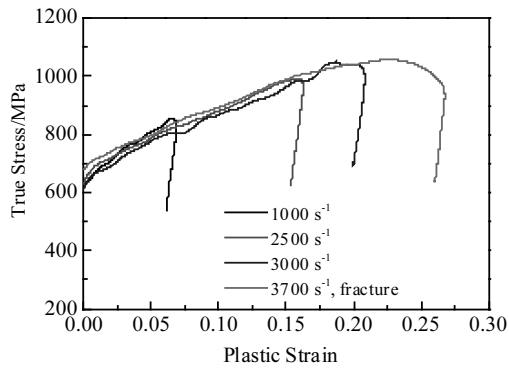


Fig.2 True stress-plastic strain curves of Ti-16V alloys compressed at different strain rates

that the adiabatic heat generated at high strain rates was not enough to alter the dominant deformation mode. Moreover, the flow stress was insensitive to the strain rate.

2.3 Microstructure observation

Fig.3 shows optical micrographs of specimens compressed at various strain rates. Equiaxed β grains were observed in water quenched Ti-16V alloy (see Fig.3a). At a strain rate of 1000 s^{-1} , lots of plate-like features were observed, as shown in Fig.3b. With an increase of strain rate, these plate-shaped features began to intersect (see Fig.3c). If the strain rate reached to 3000 s^{-1} , the ASB was activated and propagated along the 45° direction with the compressive axis in Fig.3d. Thus, the critical instability strain rate of the Ti-16V alloys was measured to be about 3000 s^{-1} . Beyond 3000 s^{-1} , crack formed and propagated along the ASB, as shown in Fig.3e.

Based on OM observations, multiple deformation products could not be still identified. The EBSD technique was further applied to observe the deformed microstructures. The sample compressed at 1000 s^{-1} was taken as an example to show the dynamic deformation feature due to a slight

lattice distortion. As shown in Fig.4a, microstructure details were exhibited clearly by the overlapping map of IPF and image quality (IQ) figure. Part of plate-like features were determined to be $\{332\}\langle 113 \rangle$ type twinning, a common twinning system in β titanium alloys^[19,20]. The coincidence site lattice of this twinning system is $\Sigma 11$ boundary^[21], corresponding to 50.5° misorientation angle around $\langle 110 \rangle$ direction as indicated in Fig.4b. Fig.4c shows the boundary of $\{332\}\langle 113 \rangle$ type twinning, which was corresponding to part of deformation products in OM observations. However, there also existed some products which could not be recognized because of the size difference with twins. Therefore, finer deformation products were further observed by TEM.

Fig.5 shows the plate-shaped feature identified as stress induced ω phase with hexagonal crystal structure according to the selected-area electron diffraction patterns, which was consistent with finer features in OM and EBSD observations. There is a discrepancy of the activation of stress induced ω phase transformation in Ti-V alloys^[9, 22], which was caused by interstitial oxygen atoms contained in materials. Wang et al found that high level of oxygen may suppress the stress induced ω phase transformation in Ti-20V alloys^[23]. Min et al reported that the oxygen content ranging from 0.1%~0.5% leads to a suppression of β phase to ω phase^[24]. In this work, the oxygen content of the experimentally used Ti-16V alloy was 0.025%, which resulted in deformation modes including twinning and stress induced ω phase transformation. Similar results were also observed in quasi-static tensile microstructures of Ti-16V alloys^[25].

2.4 Twinning activation

Twinning is resulted from the shear movement of atoms along specific direction on specific crystalline plane^[26]. The Schmid law is commonly used to predict the activation of twinning or slip. And the selection of the activated twinning variant can also be predicted by the Schmid law^[27]. For

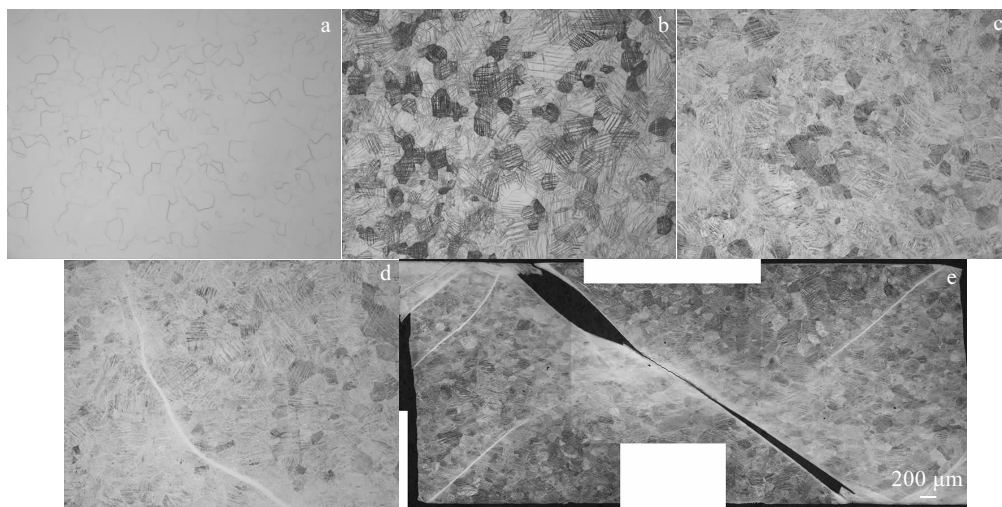


Fig.3 Optical micrographs of the undeformed specimen (a) and samples compressed at different strain rates: (b) 1000 s^{-1} , (c) 2500 s^{-1} , (d) 3000 s^{-1} , and (e) 3700 s^{-1}

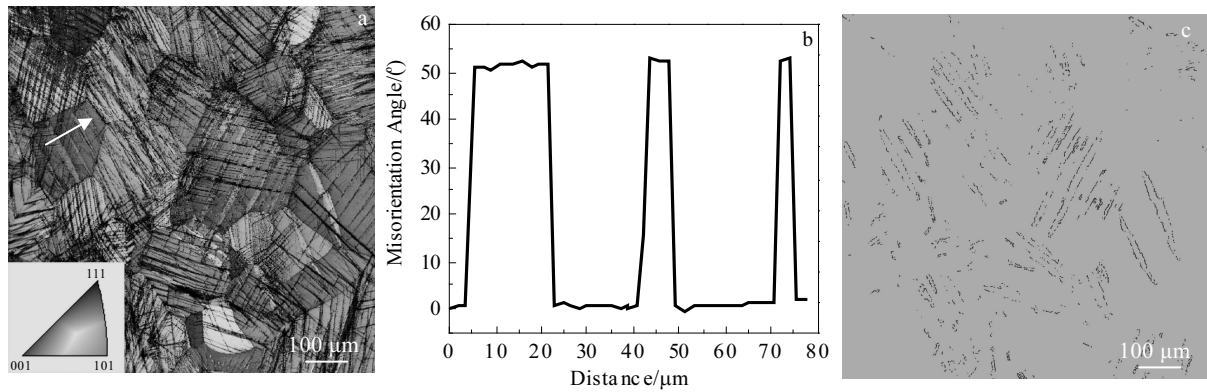


Fig.4 Overlapping map (IPF and IQ) of the specimen compressed to 0.044 (plastic strain) at 1000 s⁻¹ (a), line traces across the region arrowed in Fig.4a showing misorientation angles (b) and {332}<113> type twinning boundary map (c) (the normal direction of the observed plane is parallel to the compressive axis)

{332}<113> type twinning system, it can be activated in twelve different ways, termed variants in this research^[28]: (332)[113̄], (332)[113̄], (332)[113̄], (332)[113̄], (323)[131̄], (323)[131̄], (323)[131̄], (233)[311̄], (233)[311̄], (233)[311̄] and (233)[311̄]. In the present work, the twinning SF was defined similarly to slip as:

$$SF = \cos \Phi \cdot \cos \lambda \tag{1}$$

Φ is the angle between compressive direction and normal direction to the twinning plane; λ is the angle between compressive direction and twinning shear direction. Both are ranged in 0°~180°.

The spherical coordinate system for SF calculation with one example ((332)[113̄] variant) is presented in Fig.6. The coordinate system is established around a body centered cubic (bcc) unit cell. The axes of X, Y and Z are in accordance with <100>, <010> and <001> direction, respectively. The unit vector \overline{PO} indicates the loading direction, which is determined by the angle pair (θ , α). θ is the angle between the loading direction and the Z axis; α is the angle between the loading projection on the XOY plane (\overline{RO}) and the X axis. The ranges of θ and α are 0~180° and 0°~360°, respectively. The unit vector $\overline{P'O'}$ is parallel to the unit vector \overline{PO} . The grey surface ABC is presented as (332)

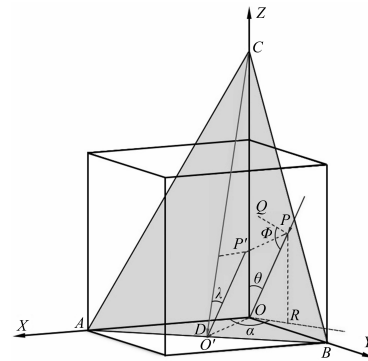


Fig.6 Illustration of the coordinate system applied to calculate the twinning SF values

twinning plane and \overline{PQ} is the normal vector of that. The twinning shear direction of [113̄] is indicated by vector \overline{CD} delineated by the red line.

According to Eqs. (1)~(6), SF values can be calculated and the results are shown in Fig.7. It is noticed that compressive direction is fixed in the EBSD analysis system but variable in the coordinate system of bcc unit cell. For a given twinning variant, the SF values of grains with different orientations can be obtained based on Fig.7. Different from slipping, negative SF values were resulted from the unidirectional twinning shear direction^[29]. The SF map of other variants can be calculated by varying $\overline{PQ}/|\overline{PQ}|$ and $\overline{CD}/|\overline{CD}|$.

$$\cos \phi = \overline{PO} \cdot \left(\frac{\overline{PQ}}{|\overline{PQ}|} \right) \tag{2}$$

$$\cos \lambda = \overline{P'O'} \cdot \left(\frac{\overline{CD}}{|\overline{CD}|} \right) \tag{3}$$

$$\overline{PO} = (-\sin \theta \cdot \cos \alpha, -\sin \theta \cdot \sin \alpha, -\cos \theta) \tag{4}$$

$$\frac{\overline{PQ}}{|\overline{PQ}|} = (0.640, 0.640, 0.426) \tag{5}$$

$$\frac{\overline{CD}}{|\overline{CD}|} = (0.302, 0.302, -0.905) \tag{6}$$

Given a specific grain orientation, it is postulated that the variant with high SF values would be activated preferentially^[27]. The maximum of SF values among all variants is

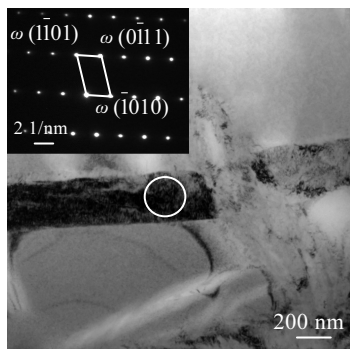


Fig.5 TEM bright-field images of stress induced ω phase in the specimen compressed at 1000 s⁻¹

defined as the SF value possessed by the twinning system, which is illustrated as the top layer in Fig.8. The black square ($0^\circ \leq \alpha \leq 45^\circ$, $0^\circ \leq \theta \leq 90^\circ$) was picked up due to the rotational symmetry of the SF map. Note that the samples were cut perpendicular to the compressive axis, indicating that the compressive axis was parallel to the ND direction set in the EBSD analysis system. According to the definition of Euler angles (φ_1 , Φ , φ_2) of grains, angle θ and α can be transformed by the Euler angle as follows:

$$\theta = \begin{cases} \Phi & \Phi \leq 90^\circ \\ 180^\circ - \Phi & \Phi > 90^\circ \end{cases} \quad (7)$$

$$\alpha = \begin{cases} \varphi_2 & \varphi_2 \leq 45^\circ \\ 90^\circ - \varphi_2 & 45^\circ < \varphi_2 \leq 90^\circ \\ \varphi_2 - 90^\circ & 90^\circ < \varphi_2 \leq 135^\circ \\ 180^\circ - \varphi_2 & 135^\circ < \varphi_2 \leq 180^\circ \\ \varphi_2 - 180^\circ & 180^\circ < \varphi_2 \leq 225^\circ \\ 270^\circ - \varphi_2 & 225^\circ < \varphi_2 \leq 270^\circ \\ \varphi_2 - 270^\circ & 270^\circ < \varphi_2 \leq 315^\circ \\ 360^\circ - \varphi_2 & 315^\circ < \varphi_2 \leq 360^\circ \end{cases} \quad (8)$$

As a result, the SF values of grains in Fig.4a can be depicted in Fig.9a. Obviously, these symbols scattered in zones with different levels of SF values. Note that twinned grains were located in regions with high SF values while untwinned grains scattered in zones with relatively low SF values. Therefore, there existed a critical SF value determining the activation of twinning. Exact SF values of grains in Fig.4a are listed in Fig.9b. The range of the critical SF value was measured to be 0.392~0.399, which was indicated by the dotted line. The critical SF value can be used to predict the activation of twinning behavior of Ti-16V alloys. If the SF value of one grain is higher than that, twinning behavior will be more possible to be activated, otherwise the grain may deform by other modes possibly. Therefore, the SF value is a key factor for predicting the deformation mode and the activation of twinning behavior has a strong relationship with the orientation of a grain.

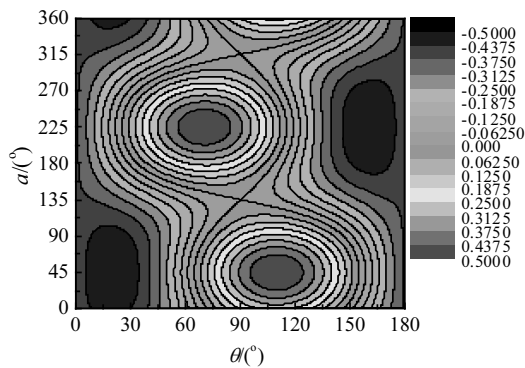


Fig.7 Calculated SF map of $(332)[\bar{1}13]$ twinning variant

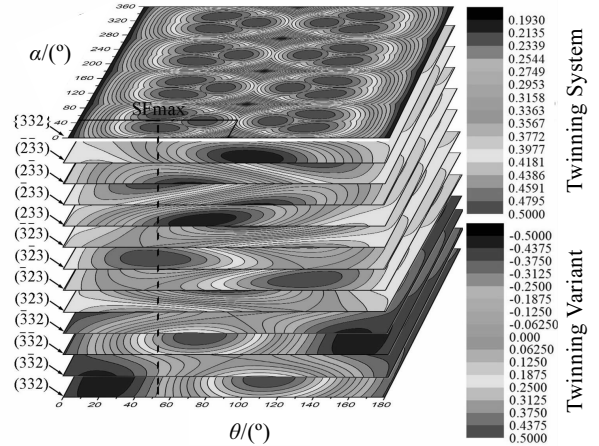


Fig.8 SF map of $\{332\}\langle 113 \rangle$ type twinning covered by twelve variants

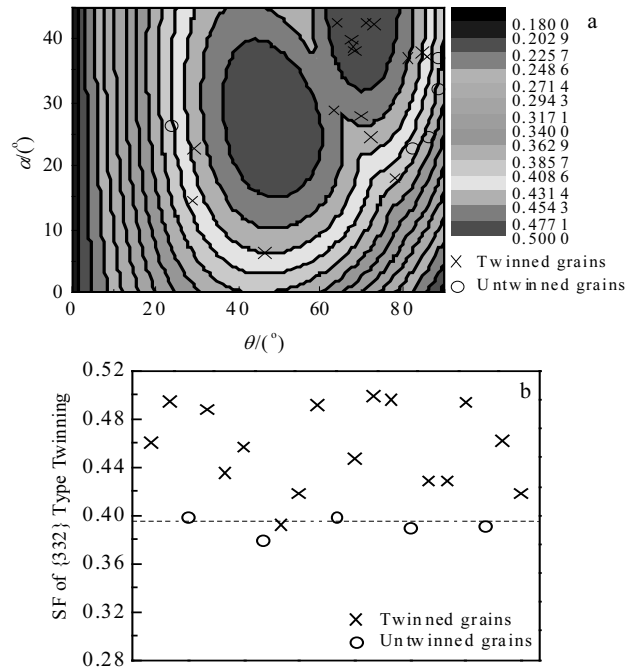


Fig.9 SF map of $\{332\}\langle 113 \rangle$ type twinning with experimentally investigated grains (a) and corresponding SF values of twinned and untwinned grains (b)

3 Conclusions

- 1) The Ti-16V alloys exhibit a pronounced strain hardening effect at high strain rates while the flow stress and strain hardening rate are insensitive to the loading strain rate.
- 2) The critical instability strain rate of Ti-16V alloys is measured to be about 3000 s^{-1} .

3) A combination of $\{332\}\langle 113 \rangle$ type mechanical twinning and stress induced ω phase transformation are verified to be dominant dynamic deformation modes of Ti-16V alloys.

4) Schmid factor is a key parameter determining the activation of the twinning behavior of Ti-16V alloys.

References

- Al-Zain Y, Kim H Y, Koyano T et al. *Acta Materialia*[J], 2011, 59(4): 1464
- Xing H, Sun J, Yao Q et al. *Applied Physics Letters*[J], 2008, 92(15): 151 905
- Miyazaki S, Kim H Y, Hosoda H. *Materials Science and Engineering A*[J], 2006, 438-440: 18
- Williams D N, Wood R A, Bartlett E S. *Metallurgical Transactions*[J], 1972, 3(6): 1529
- Zhan H Y, Wang G, Kent D et al. *Acta Materialia*[J], 2016, 105: 104
- Abdel-Hady M, Hinoshita K, Morinaga M. *Scripta Materialia*[J], 2006, 55(5): 477
- Yang Y, Li G P, Cheng G M et al. *Applied Physics Letters*[J], 2009, 94(6): 061 901
- Kuan T S, Ahrens R R, Sass S L. *Metallurgical Transactions A*[J], 1975, 6: 1767
- Oka M, Taniguchi Y. *Metallurgical Transactions A*[J], 1979, 10(5): 651
- Hanada S, Izumi O. *Metallurgical Transactions A*[J], 1986, 17(8): 1409
- Wang X L, Li L, Mei W et al. *Materials Characterization*[J], 2015, 107: 149
- Koul M K, Breedis J F. *Acta Metallurgica*[J], 1970, 18(6): 579
- Hokka M, Leemet T, Shrot A et al. *Materials Science and Engineering A*[J], 2012, 550: 350
- Khosravifard A, Moshksar M M, Ebrahimi R. *Materials and Design*[J], 2013, 52: 495
- Ahmed M, Gazder A A, Saleh A A et al. *Metallurgical and Materials Transactions A*[J], 2017, 48(6): 2791
- Zhang Z H, Liu Q M, Yang H Y et al. *Journal of Materials Engineering and Performance*[J], 2017, 26(7): 3368
- Shin S, Zhang C, Vecchio K S. *Materials Science and Engineering A*[J], 2017, 702: 173
- Chichilia D R, Ramesha K T, Hemkera K J. *Acta Materialia*[J], 1998, 46(3): 1025
- Tobe H, Kim H Y, Inamura T et al. *Acta Materialia*[J], 2014, 64: 345
- Zhou X Y, Min X H, Emura S et al. *Materials Science and Engineering A*[J], 2017, 684: 456
- Min X H, Chen X J, Emura S et al. *Scripta Materialia*[J], 2013, 69(5): 393
- Hanada S, Yoshio T, Izumi O. *Transactions of the Japan Institute of Metals*[J], 1986, 27(7): 496
- Wang X L, Li L, Xing H et al. *Scripta Materialia*[J], 2015, 96: 37
- Min X H, Bai P F, Emura S et al. *Materials Science and Engineering A*[J], 2017, 684: 534
- Wang X L, Li L, Mei W et al. *Materials characterization*[J], 2015, 107: 149
- Christian J W, Mahajan S. *Progress in Materials Science*[J], 1995, 39(1-2): 1
- Bertrand E, Castany P, Péron I et al. *Scripta Materialia*[J], 2011, 64(12): 1110
- Min X H, Tsuzaki K, Emura S et al. *Materials Science and Engineering A*[J], 2013, 579: 164
- Martin É, Capolungo L, Jiang L et al. *Acta Materialia*[J], 2010, 58(11): 3970

一种亚稳型 β 钛合金在高应变率下的多种变形机制

王翹楚, 惠松骁, 叶文君, 刘 睿, 于 洋

(北京有色金属研究总院 有色金属材料制备加工国家重点实验室, 北京 100088)

摘要: 以二元 Ti-16V 合金为研究对象, 采用霍普金森压杆装置、光学显微镜、电子背散射衍射技术以及透射电子显微镜, 分别测量并分析了高应变率下 Ti-16V 合金的动态力学性能、微观组织演变以及塑性变形机制。得出如下结论: Ti-16V 合金的流变抗力与应变硬化速率对应变率不敏感; Ti-16V 合金的临界失稳应变率约为 3000 s^{-1} ; $\{332\}\langle 113 \rangle$ 型孪生与应力诱发 ω 相变为 Ti-16V 合金高应变率下的主导塑性变形机制; 通过本研究构建的孪生 Schmid 因子计算模型, 定量核算与模拟 $\{332\}\langle 113 \rangle$ 型孪生的 Schmid 因子, 结合实验结果表明 Schmid 因子是决定晶粒是否发生孪生的重要参数。

关键词: 亚稳 β 钛合金; 动态变形; 变形机制; 孪生

作者简介: 王翹楚, 男, 1990 年生, 博士, 北京有色金属研究总院有色金属材料制备加工国家重点实验室, 北京 100088, 电话: 010-60662663, E-mail: 13021969461@163.com